Materials and Design 162 (2019) 60–69

Contents lists available at ScienceDirect

Materials and Design

journal homepage: www.elsevier.com/locate/matdes

The construction and performance of multi-level hierarchical hydroxyapatite (HA)/collagen composite implant based on biomimetic bone Haversian motif

Tierong Bian [a,b], Kang Zhao [a,*], Qingnan Meng [a], Yufei Tang [a], Hua Jiao [a], Jing Luo [a]

[a] School of Materials Science and Engineering, Xi'an University of Technology, Xi'an 710048, China
[b] Medical Experimental Center, The Affiliated Hospital of Southwest Medical University, Luzhou 646000, China

HIGHLIGHTS

- A prospective breakthrough made in biomimetic bone scaffold
- Biomimetic bone Haversian microstructure HA/collagen composite scaffold was prepared.
- The structure supports the mineralized scaffolds mechanical properties dual reinforcement.
- The bionic bone Haversian microstructure scaffold has popular biological properties.

GRAPHICAL ABSTRACT

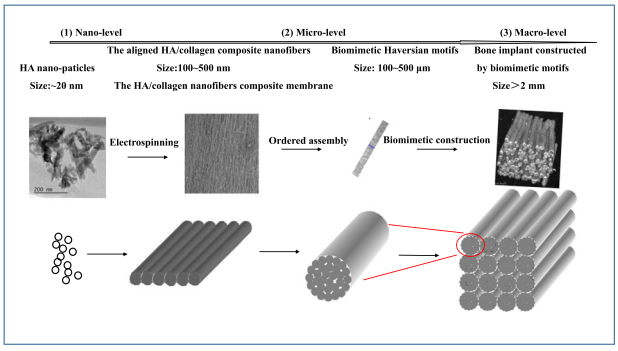

ARTICLE INFO

Article history:
Received 20 August 2018
Received in revised form 17 November 2018
Accepted 17 November 2018
Available online 18 November 2018

Keywords:
Hierarchical microstructure
HA/collagen biomimetic implant
Rolling motifs
Mechanical properties
Biocompatibility

ABSTRACT

Synthetic materials allow easy processing and modification for bone defect repairing with a good immunological compatibility and minimal risks of infections and donor site morbidity. But compared with an autologous bone graft, these artificial scaffolds still have limitations in terms of the osteogenic capacity and mechanical properties including excellent strength and toughness of super-light natural bone. In this study, we aimed to construct a bone scaffold with both a biomimetic multi-level hierarchical structure and similar constituents of a natural bone using HA/collagen composite nanofibers. The electrospinning technique and rolling method were used for bottom-up synthesis of this artificial system from nano-level to micro-level and then to macro-level. MicroCT scanning and scanning electron microscopy confirmed successful preparation of the bone scaffold composed of fully assembled microscopic fibers. The mechanical properties of the mineralized scaffolds were double reinforced by a large number of newborn HA nano particles and the chemical bonds. The bonds were formed between HA and collagen within and between the layers of the scaffold's matrix membrane. The scaffold showed an excellent biocompatibility profile. These suggest the scaffold potential for use in bone tissue engineering.

1. Introduction

Repairing a large bone defect often requires the use of implants, which can be an autologous bone graft, an allogeneic bone graft, or an artificial one [1,2]. Autologous and allogeneic bone grafts are inevitably

* Corresponding author.
E-mail address: kzhao@xaut.edu.cn (K. Zhao).

https://doi.org/10.1016/j.matdes.2018.11.040

associated with donor site surgeries and can be exposed to potential risks of pathogen transmission and immune rejection [3,4]. Tissue-engineered implants using synthetic materials exhibit great advantages for bone defect repair, but currently such artificial bones have inherent limitations in their biocompatibility, biological activity, biodegradability and mechanical compatibility to the host bones [5–7]. Therefore, the goal of bone tissue engineering is to find a biomimetic implant that is more consistent with human bone in composition, structure, function and performance.

In the field of biomimetic bone implant materials, calcium phosphate ceramics such as hydroxyapatite (HA) are widely used for constructing artificial bone scaffolds due to their similarity in inorganic composition to a human bone [8]. HA can be prepared into scaffolds with a three-dimensional porous structure to promote seed cell ingrowth and transmission of nutrients and metabolites [9]. Nevertheless, scaffold porosity is inversely correlated with its strength [10], thus this porous material can only be used for non-load-bearing bone replacement and filling bone defects [11]. Deville et al. [12] attempted to improve the compression strength of HA scaffolds by creating a directional porous structure using directional freeze-drying technique, but the modified scaffold was still not as strong as natural bones.

The properties of human bone are determined by complex composition, macroscopic structure and precise microstructure. Human bone is composed of nanoscale apatite, collagen and other trace elements, and its microstructure is characterized by bone Haversian motifs, the super microstructure units is composed of mineralized collagen fibers [10,13–17]. In recent years, many scholars have conducted biomimetic preparation of human bone composition and nano structure. Deville et al. [12,18,19] revealed directional frozen suspension for ceramics, using the microstructure of ice as a framework of template to produce layered pores and layered crystals with a width from one to several hundred microns, which resulted in much enhanced strength (by nearly 3 folds) compared to that of conventional materials. The recent advancement in 3D printing, drop deposit printing, laser pulse, and UV 3D imaging makes possible the fabrication of composite scaffolds with complex structure of a customized design [20–26]. Gorodzha et al. [27,28] reported that the randomly oriented and well-aligned microfibers scaffold simulates the extracellular matrix of bone tissue, reveal good cells adhesion and proliferation. Hydrophilic SiHA nanoparticles improve tissue growth, and piezoelectric poly(3-hydroxybutyrateco-3-hydroxyvalerate) (PHBV) demonstrates good calcium deposition. However, the bone scaffolds does not have the advantages of simulating multi-level hierarchical natural bone structure (the structure with extraordinary properties) and nano component of bone (collagen and nano HA, natural bioactive components), and the organic component of the bone scaffolds is non-hydrophilic and has poor degradation performance [29]. Shao et al. [30] demonstrated that electrospun multi-layer nanofibers scaffold simulating the hierarchical structure of bone collagen fibers resulted in excellent mechanical properties and biocompatibility. The scaffolds prepared by layer-by-layer rolling or cross-linking homogeneous/heterogeneous spinning nanofiber membrane could improve the cell compatibility and mechanical properties [31–34].

In spite of these advancements, the microstructure, composition and properties of the currently artificial materials are far from ideal when compared to the human bone. In this study, we aimed to develop a new bone substitute similar to natural bone in both composition and microstructure using aligned HA/collagen composite nanofibers, which were hierarchically assembled in a bottom-up fashion to simulate the natural human bone structure at the nano-, micro- and macro-level. The mimic multi-level hierarchical artificial bone scaffold rarely reported. Finally, it is desired that the bone scaffold can show excellent mechanical properties and biocompatibility which make it an ideal biomimetic implant for tissue engineering.

2. Materials and methods

2.1. Preparation of HA/collagen nanofiber biocomposite

The sol-gel solution was prepared by dissolving 1.18 g polyvinylpyrrolidone (PVP) (molecular weight of 1.3×10^5 g mol^{-1}; provided by Aladdin Industrial Co., China) in 10 mL absolute ethyl alcohol. HA nanoparticles with a diameter of around 20 nm. 1.18 g HA (provided by Nanjing Epui Nanometer Material Co. Ltd., China) were dispersed in 10 mL absolute ethyl alcohol and sonicated for 30 min twice. The prepared HA suspension was mixed with PVP sol-gel solution, stirred with a magnetic stirring apparatus, and sonicated for 30 min twice to obtain a stable and homogeneous spinning solution, which was then electrospun in an electrostatic spinning apparatus with a rotating cylinder as the collector. The cylinder rotation speed was 2700 rpm, and the electrospinning was carried out at a voltage of 20 kV, a flow rate of 0.05 mL h^{-1} and a receiving distance of 12.5 cm). The membrane was then calcined at 550 °C for 2 h to obtain the HA nanofibers. The fibers were immersed in a solution containing 64 mg/mL collagen (Sichuan Mingjean Biotechnology Co. Ltd., China) for 2 times, and the HA/collagen nanofiber biocomposite obtained were cross-linked for 24 h in the presence of 25% glutaraldehyde.

The HA/collagen nanofiber membrane was soaked in 10× simulated body fluid (SBF, prepared according to the protocols described by Tas et al. [35]), which was changed every 2 h. After 6 h, the membrane was taken out, washed with distilled water for 3 times, and then dried at 37 °C. The ultrastructure of the membrane was observed using scanning electron microscopy (SEM) coupled with energy-dispersive spectroscopy (EDS) analysis (JEOL JSM-6700F microscope, Zeiss, Germany).

2.2. Construction of multi-level hierarchical HA/collagen composite implant

To construct the multi-level hierarchical HA/collagen composite implant with biomimetic bone Haversian motif, the fibers were first aligned in parallel by electrospinning technique, and the aforementioned composite fiber membrane composed of nanoscale raw HA and collagen were rolled (parallel to the fibers axial) to form the biomimetic bone motifs (500 μm in diameter), which contained 3 bottom-up hierarchical levels: raw materials of HA and collagen (nanoscale), HA/collagen fibers (nanoscale), and composite fiber membrane (microscale). The motifs (the 4th, or the microscale, level of the bone) were paralleled in its axial direction to construct bone Haversian system (5 mm in diameter, macroscale) as the bone scaffolds, which mimicked the hierarchical structure of the natural bone [13,16,17,36,37].

2.3. Characterization of biomimetic bone scaffold microstructure

The constructed bone scaffold was scanned with micro-computed tomography (microCT) (Siemens Inveon 3125). The resultant datasets were evaluated for the micro-architectural parameters in an Inveon research workplace including the scaffold volume (SV), material volume (MV) of the scaffold, pore size, and the distribution and specific surface area (SS/SV). The porosity analyzed with Inveon research workplace was derived using Eq. (1).

$$\text{Porosity}\% = (\text{SV}-\text{MV})/\text{SV} \times 100\% \quad (1)$$

The cross-sectional and three-dimensional morphology of the scaffold was observed with microCT.

To analyze the fine microscopic structure of the bone scaffold, the transverse and longitudinal sections of the bone scaffolds were magnified step-by-step. To characterize the longitudinal section morphology and microstructure, the motif of the scaffold was torn apart, immersed it in liquid nitrogen for 15 min.

2.4. Mechanical property assessment of the bone scaffold

According to the standard specimen size range for compression test recommended by Keaveny et al. [38–40], we prepared the scaffolds into φ6 mm × 12 mm specimens. The mechanical properties of the scaffolds were tested using a high-temperature electronic testing machine at a compression speed of 0.5 mm/min. To assess the stability of the bone scaffold in vivo, we soaked the bone scaffolds in 10 × SBF for 1, 2, or 6 h to simulate the mineralization in vivo before testing the mechanical properties; for each soaking time (including 0 h), the compression test was repeated for 5 times and the compressive strength, Young's modulus and the strength corresponding to the strain of the samples were all analyzed. For convenience of description in the following text, we coded the scaffold specimens soaked in 10 × SBF for 0 h, 1 h, 2 h, and 6 h as 1#, 2#, 3# and 4#, respectively.

2.5. Biocompatibility assessment of the bone scaffolds

The bone scaffolds were cut into small pieces (6 mm in diameter) and irradiated with short-wavelength UV-light for 30 min, sterilized with 70% ethanol overnight, and washed with phosphate buffer saline (PBS) for 3 times. Mesenchymal stem cells (MSCs) were cultured at 37 °C in Dulbecco's modified Eagle medium (DMEM; Gibco, USA)) supplemented with 10% (V/V) fetal bovine serum (FBS) in a humidified atmosphere containing 5% CO_2. The media was changed every other day. After 7 days of culture, the monolayer MSCs were detached with Trypsin-EDTA to prepared the single cell suspensions. The viable cells were counted with a hemocytometer and resuspended in the medium containing 5% FBS at the final density of 2×10^5 cells/mL. The MSCs were seeded in a 6-well cell culture plate at 4×10^5 cells/well in 2 mL of DMEM supplemented with 10% FBS and incubated with the bone scaffolds at the bottom of the wells at 37 °C, with the cells cultured in the absence of the scaffold as control.

After 72 h of incubation, the scaffolds were removed and washed twice with cold PBS; the cells adhering to the scaffolds were fixed by immersing the scaffolds in PBS containing 2.5% (V/V) glutaraldehyde for 10 min followed by washing with PBS for 3 times. The scaffolds were carefully placed on glass slides, air dried, stained with 4′,6-diamidino-2-phenylindole, dihydrochloride (DAPI), and observed with laser scanning confocal microscope (Carl Zeiss, Jena, Germany) [41]. A second set of scaffold specimens were further dehydrated in gradient ethanol of 50%, 60%, 70%, 80%, 90%, and 100%, for 15 min for each concentration, dried overnight, and observed under SEM [42].

For CCK8 assay, the scaffold samples were leached (ISO 10993-12:2012, Biological Evaluation of Medical Devices) with DMEM containing 10% FBS for three days before the experiment. The leach solutions were blended every day and stored at 4 °C until use. The cells were seeded in triplicate in 96-well plates (100 μL per well) at a plating density of 1×10^4 cells/well and incubated to allow for cell attachment. After 24 h, the culture medium was removed and the cells were cultured with 100 μL of 100% leach liquor for 24, 48, or 72 h. The wells containing 100% leach solution but no cells served as the blank control, and the cells cultured in the culture medium without the leach solution as the positive control. After the incubation, 10 μL of CCK8 solution was added to each well, and the plate was incubated at 37 °C for 2 h before measurement of the optical absorbance (OA) at 450 nm using a full-wavelength spectrophotometer (Thermo Fish Co. Ltd., Germany). The relative growth rate (RGR) of the cells was quantified by optical absorbance (OA) (450 nm) using the following equation:

$$RGR\% = |OA|_{Experimental} / |OA|_{Control} \times 100\%$$

The toxicity of the scaffold material was classified into 5 grades according to RGR: no toxicity (a RGR above 100), grade 1 toxicity (a RGR between 99 and 75), grade 2 toxicity (a RGR between 74 and 50), grade 3 toxicity (a RGR between 49 and 25), grade 4 toxicity (a RGR between 25 and 1), grade 5 toxicity (a RGR less than 0) [43].

3. Results and discussion

3.1. Morphology, cross-linking and biomineralization of the nanofiber membrane

The morphology of the aligned HA/PVP nanofiber membrane was shown in Fig. 1a. The uniform nanofibers were basically parallel to each other. The membrane was calcined and used as the nanofiber skeleton for preparing HA/collagen composite. Fig. 1b–d show the aligned HA/collagen nanofiber membrane after cross-linking and biomineralization. Glutaraldehyde cross-linking did not affect the intrinsic chemical structure of the native collagen or HA [44] and maintained the biological activities of HA and collagen in the composite. As shown in Fig. 1c, the nanofibers were coated with fine and dense biomineralization products, which enhanced the membrane strength. The product had an atomic ratio of Ca/P about 1.37 (Fig. 1d), similar to the composition of HA in human bones [45].

3.2. Bottom-up construction of the biomimetic scaffold

The process of the biomimetic scaffold construction is illustrated in Fig. 2. The current studies of biomimetic bone scaffolds focus mainly on simulation of the porous bone structure (multistage gradient pores [23], directional through-pores [19], etc.) and improvement of the strength of the graft (by cross-linking [46], rolling nanofibers [34] and weave fibers [30], etc.). Based on the above design method, the work is not only from the perspective of bone composition but also bone microstructure, including nanometer level (nano scale raw materials and nanofibers), micron level (nanofibers membrane and biomimetic motifs), and macroscope level (biomimetic bone plants). We mimic the multi-level hierarchical structure of natural human bone step-by-step. The structure bone scaffold had an optimal collagen to HA mass ratio of 57.55/42.45.

3.3. MicroCT and structural characterization of the scaffold

Fig. 3 presents the microCT morphology of the implant. The sections and stereogram show that the biomimetic bone consists of motifs similar to the actual anatomy of natural bones [42]. The structural parameters of HA/collagen composite implant are listed in Table 1. The porosity of the scaffold was 39.23 ± 0.43% by microCT (total porosity) and 34.45 ± 0.39% by Archimedes method (open porosity). The open/total porosity was about 87.82%, which could facilitate cells adhesion and promote cells growth and metabolism. The specific surface area of the scaffold was 47.40 ± 2.12 m^2/m^3, and this large specific surface area may promote vascularization and cellular infiltration [47].

3.4. Microstructure SEM analysis of the motifs composed HA/collagen implant

Microstructural observation with SEM of the composite HA/collagen implant on the transverse section (Fig. 4) and the longitudinal section (Fig. 5) showed the presence of lamellar cylindrical motif in the scaffold, highlighting concentric lamellations in the motif (Fig. 4a) with straight-through gaps between the layers ranging from 40 μm to 50 μm (Fig. 4b), which could expand the contact area of the scaffold with body fluid to facilitate the degradation and mineralization of the implant. SEM at a higher magnification revealed a clear pattern of arrangement of the nanofiber (Fig. 4c) and the nanoparticles that made up of each fiber (Fig. 4d).

SEM of the longitudinal section of the scaffold revealed the parallel alignment of the nanofibers and the biomimetic bone structure at the nanoscale and micro- and macroscopic levels (Fig. 5). The scaffold

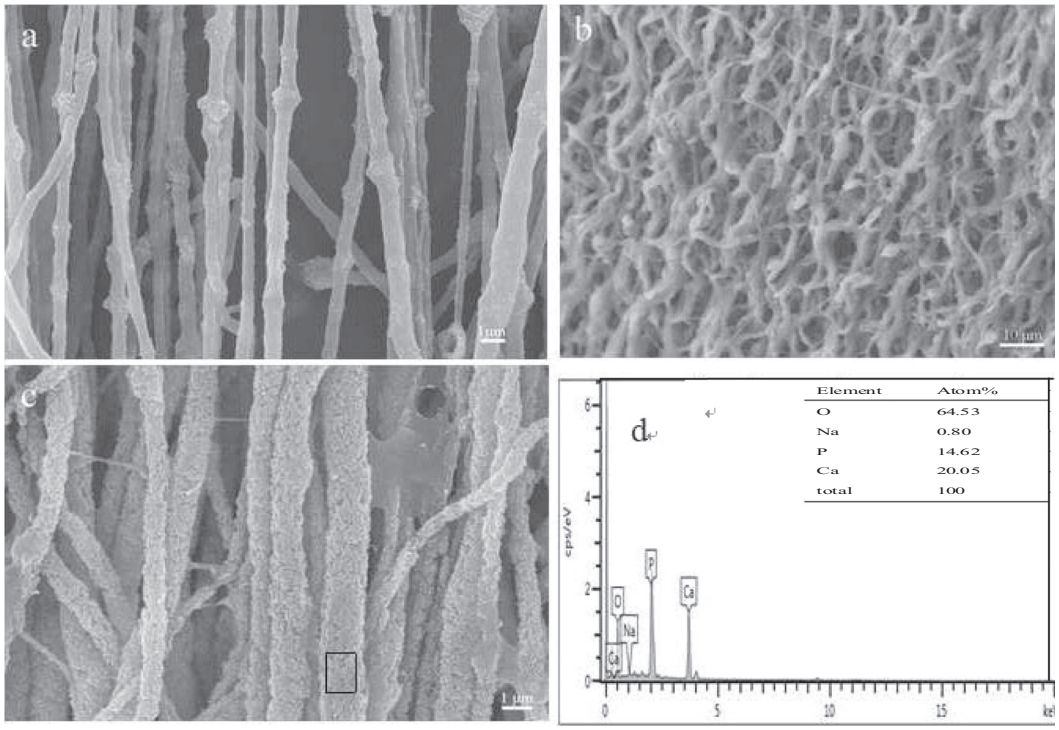

Fig. 1. Scanning electron microscopic (SEM) images of aligned composite nanofibers. (a, Aligned HA/PVP nanofibers. b, HA/collagen nanofibers after glutaraldehyde cross-linking. c, Biomineralized nanofibers in 10 × SBF. d, Composition of the biomineralized product).

implant we constructed had the expected structure resembling the hierarchical structure of a natural bone [13].

3.5. Mechanical properties of the bone scaffolds

As shown in Fig. 6, the compressive strength of samples 1#, 2#, 3# and 4# were about 3, 10, 19 and 22 MPa, respectively. The substantial increments of the compressive strength as the soaking time in SBF increased was attributed to the formation of HA during continuous soaking time in SBF increased was attributed to the formation of HA during continuous mineralization process (Fig. 1c, d). The Young's modulus of samples 1#, 2#, 3# and 4# were approximately 19, 165, 335 and 360 MPa, respectively, demonstrating significant increments in Young's modulus of samples after soaking in SBF for 1, 2, and 6 h (by 8.6, 17.6, and 18.9 folds relative to the sample without SBF treatment, respectively). The compressive strength corresponding to strain were about

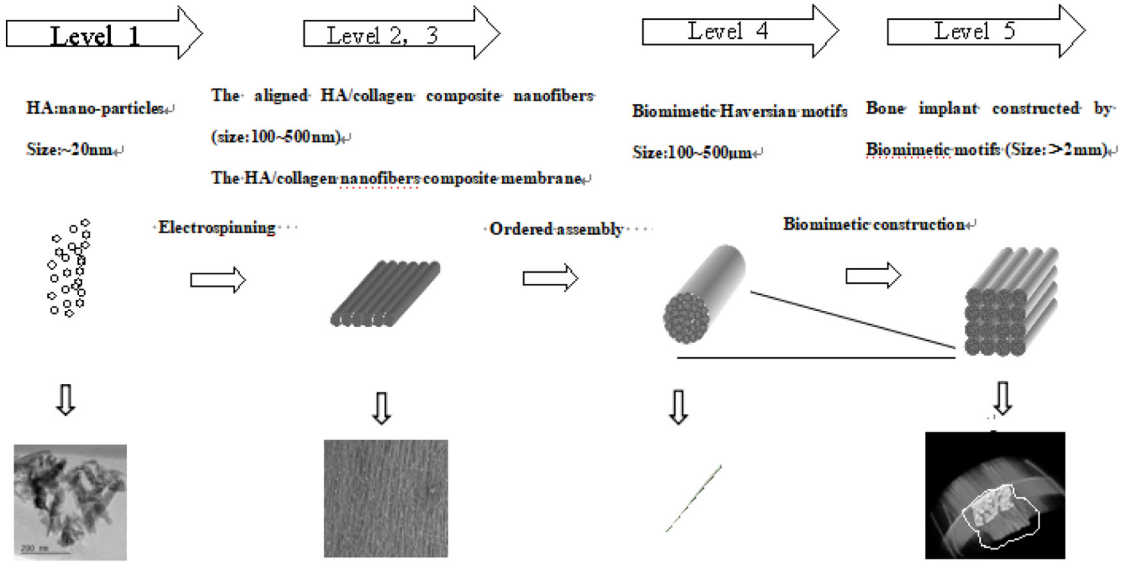

Fig. 2. Multi-level hierarchical structure schematic diagram of HA/collagen composite implant (a composite implant that is assembled step by step; the microstructure is similar to the human bone constituent unit which has a hierarchy of multiple levels).

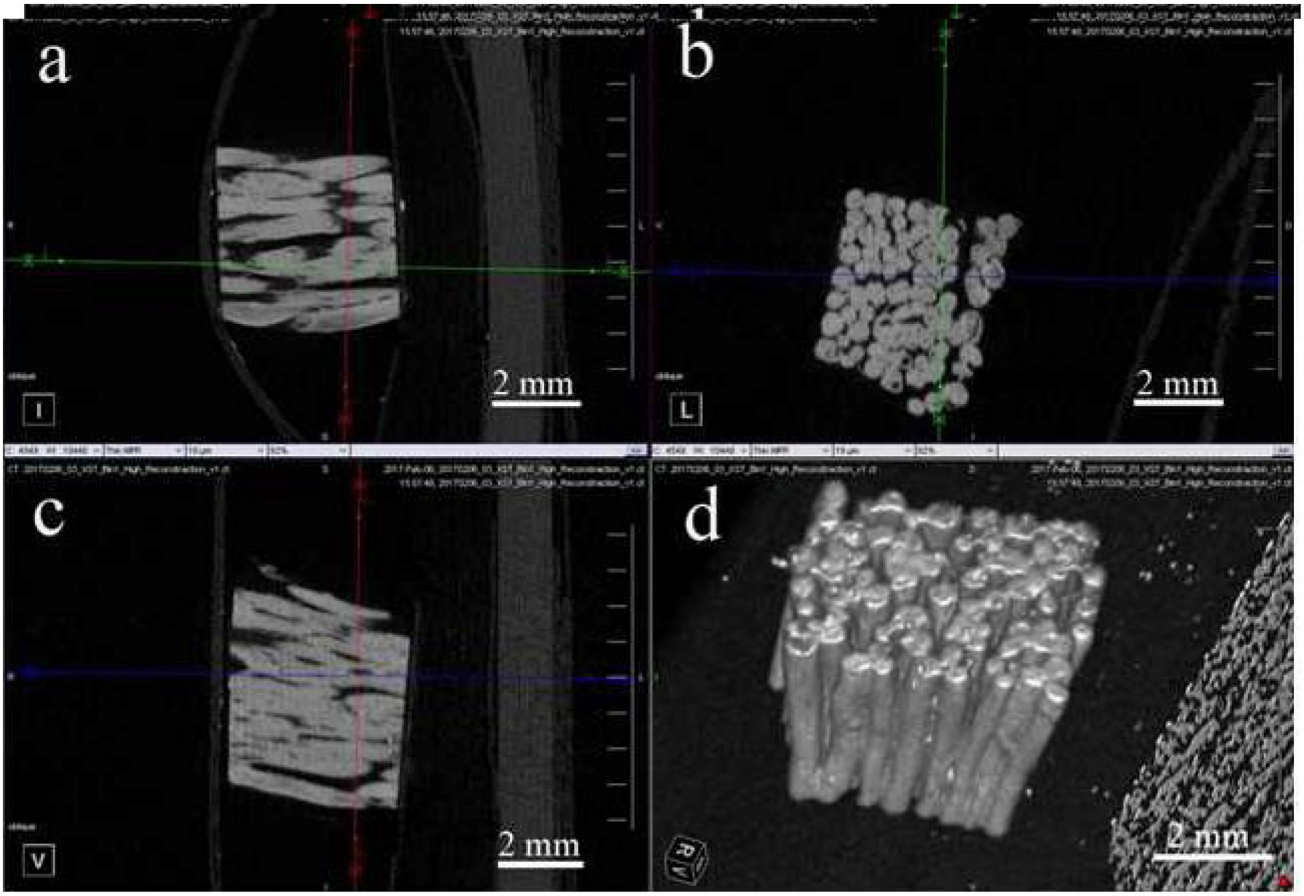

Fig. 3. MicroCT scanning of the longitudinal and cross sections and three-dimensional topography of HA/collagen composite implant. (a, Longitudinal section. b, Cross section. c, Oblique section. d, Stereogram).

only 16%, 6%, 8% and 6% for the 4 samples, respectively, suggesting that a small strain caused a rapid increase in compression resistance, as the positive effect of Haversian microstructure and HA. The compressive strengths and Young's modulus of the scaffold were greatly improved after soaking in SBF in a time-dependent manner, possibly because of the biomineralization of the collagen component triggered by calcium and phosphate ions in the SBF through a mechanism similar to that described by Shin et al. [48]. As a result, HA was formed and distributed along the composite nanofibers to reinforce the strength of the scaffolds.

In addition, collagen is rich in amide groups, which can form chemical bond with HA [49]. The scaffold had a large specific surface area and an interpenetrating porous structure to allow SBF circulation, thus abundant HA was generated and bonds were formed among HA and collagen, fibers, membrane layers and biomimetic bone motifs, resulting in much enhanced mechanical properties of the scaffold. The strains corresponding to the compressive strength of the samples were all not higher than 16%, which was consistent with the loading strain of no more than 8% in natural bones; a loading strain over 16% may likely result in fracture [50,51].

According to the available reports, when compared to the mechanical properties of the scaffolds reported, the scaffold simulating multi-level hierarchical bone structure, its initial compression strength is 3 MPa, better than that of mimic honeycomb structure bone scaffold (1.62 MPa) [52].and that of self-assembly-induced 3D plotting for macro/nano-porous collagen scaffolds with nanofibrous collagen filaments (0.35 MPa) [53]. Moreover, the compression strength of multi-level hierarchical bone scaffold before and after mineralization (the mineralization time only 6 h) are 3 and 22 MPa respectively, mineralized Young's modulus is 18.9 folds of initial modulus. While the compression strength of the bovine gelatin electrospun scaffold before and after mineralization (the mineralization time 7 days) are 2.8 and 6.3 MPa separately [54], and mineralized biomimetic collagen/alginate/silica composite scaffolds is only 2.4 folds of initial modulus [55]. The above results show that the excellent properties of the biomimetic multi-level hierarchical bone structure were not only demonstrated, but also the mechanical properties of the mineralized scaffold were also greatly improved.

Table 1
Microstructural parameters of HA/collagen composite implant.

The scaffold	
Microstructure parameters	HA/collagen composite implant
Total porosity (%) (μCT)	39.23
Open porosity (%) (Archimedes method)	34.45
Open porosity/Total porosity (%)	87.82
The specific surface area (m^2/m^3)	47.40

3.6. Biocompatibility of biomimetic bone scaffolds

We used SEM and CCK-8 assay to assess the biocompatibility of the scaffold by observing MSC growth on the scaffold implant. After culture for 3 days on the implant, numerous MSCs were attached to the

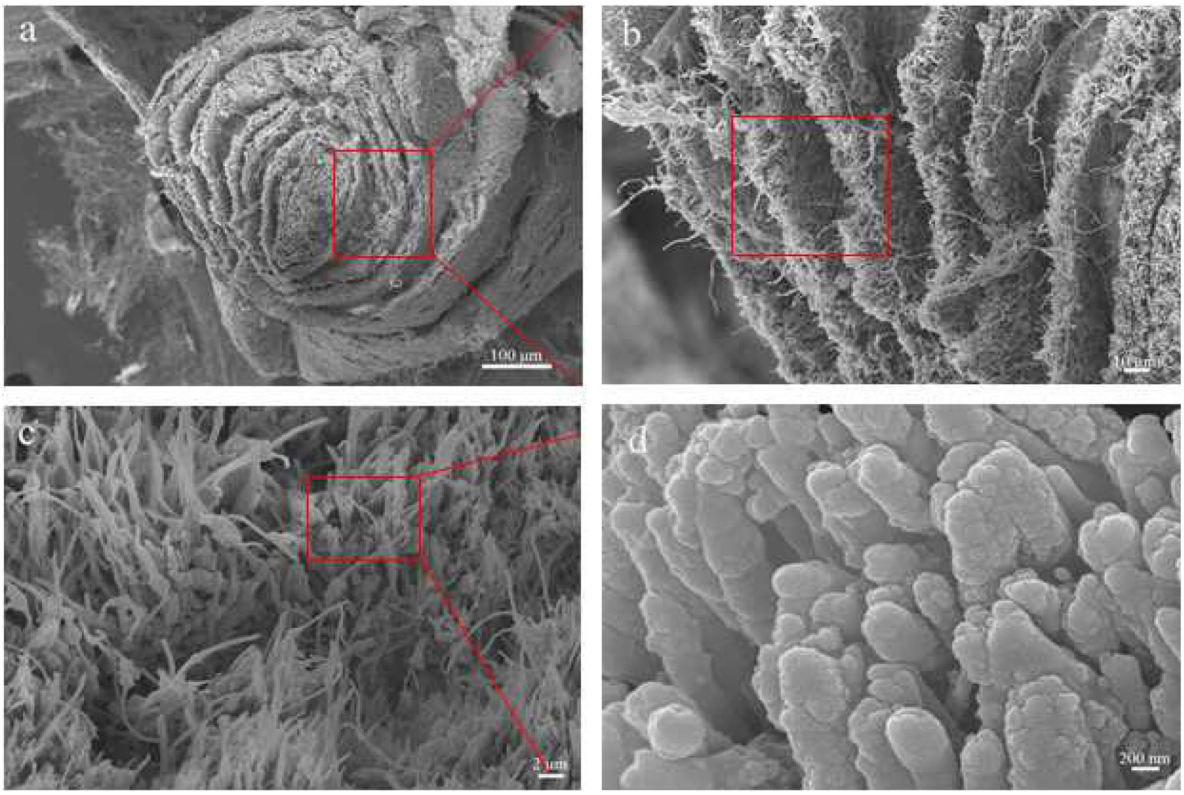

Fig. 4. SEM images of the transverse sections of biomimetic Harversian bone motif. (a, A general view of the motif. b, Interlayer morphology. c, Cross-section of the fibrous layer. d, Nanostructure of the fibers).

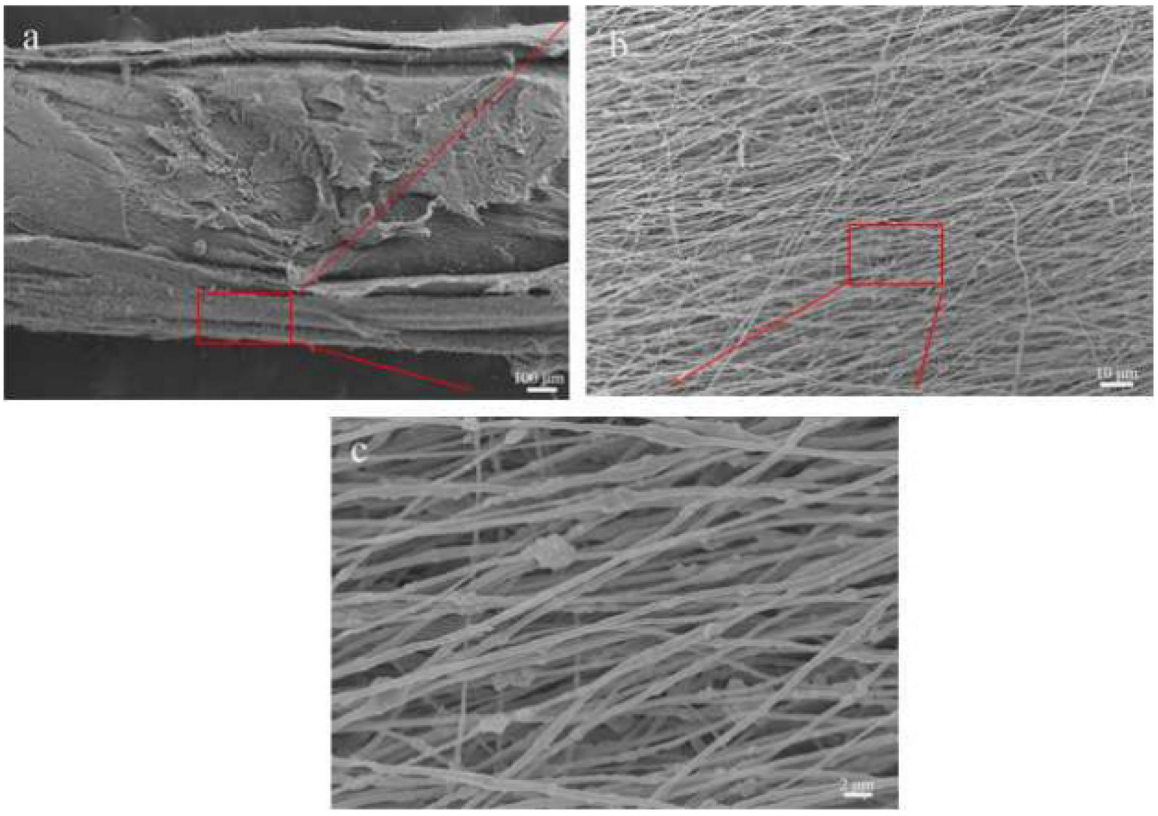

Fig. 5. SEM images of the biomimetic Harversian bone motif on the longitudinal section. (a, SEM image showing longitudinal alignment of the motif. b, Nanofibers aligned in parallel along the motif. c, Nanostructure of the fibers).

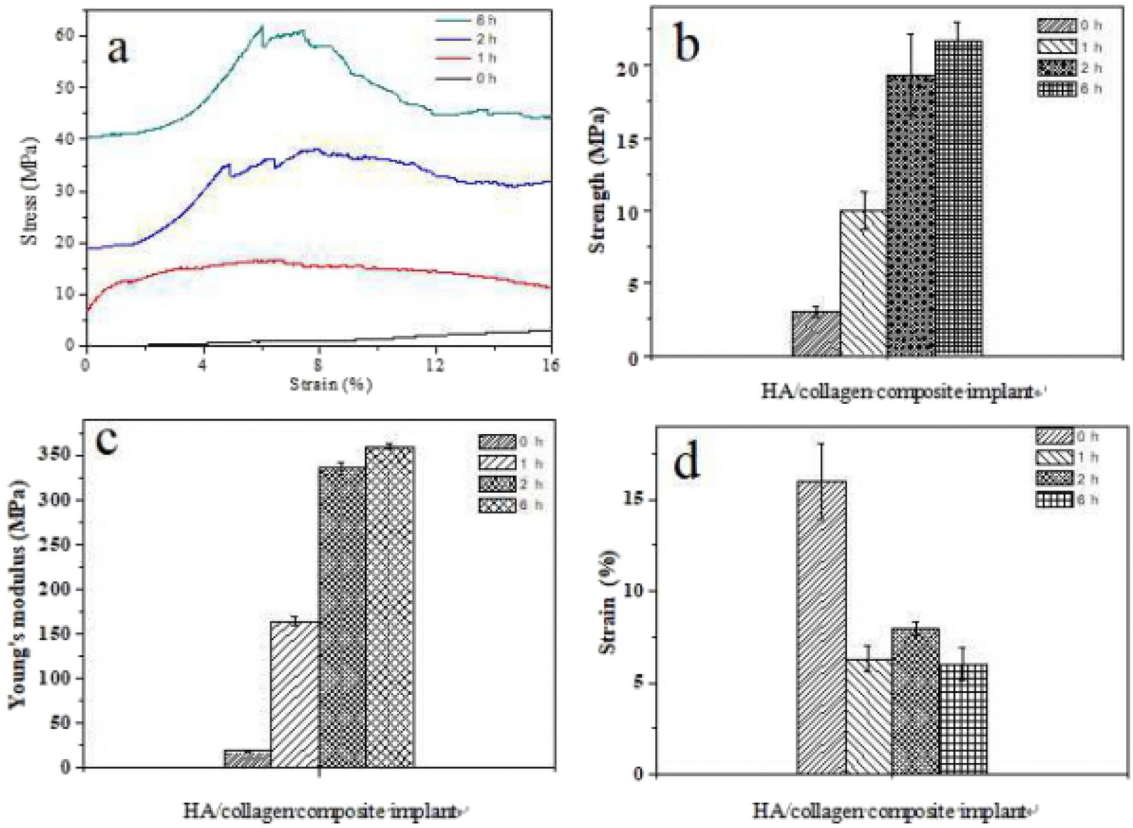

Fig. 6. Mechanical characterization of HA/collagen composite implant soaked in 10 × SBF for 0 h, 1 h, 2 h, and 6 h. (a, Stress-strain curve. b, Compressive strength. c, Young's modulus. d, Strain corresponding to compressive strength).

composite membranes (Fig. 7). The adhering MSCs showed elongation and stretching with an optimal distribution over the implant, suggesting the HA/collagen composite implant had a good biocompatibility and could well support cell growth [56,57].

We also observed the growth of MSCs seeded onto the implant using confocal microscopy. After 3 days of incubation, a large number of cells with blue nuclei were observed with a regular distribution over the HA/collagen nanofibers (Fig. 8). DAPI staining showed that the cells on the implant and the control cells had similar morphologies of the cell nuclei, suggesting the cell-friendliness of the HA/collagen nanofiber implant.

The results of CCK-8 assay showed that higher absorbance of the HA/collagen nanofibers implant at different time intervals (24, 48 and 72 h) was shown (Fig. 9), confirming that the implant leach liquor enhanced the cellular proliferation. Moreover, the cytotoxity of HA/collagen nanofibers composite implant was listed in Table 2. The cytotoxity of leach liquor in 24 h,48 h and 72 h was below 1 grade, within the realm of medical use. Overall, regardless of cell adhesion, vitality and the cytotoxicity of HA/collagen nanofibers implant, the biocompatibility of HA/collagen nanofibers implant is in the favor of bone tissue engineering.

3.7. Limitations and prospect

In spite of the many advantages, we found that the composite HA/collagen nanofiber scaffold had still insufficient compressive property

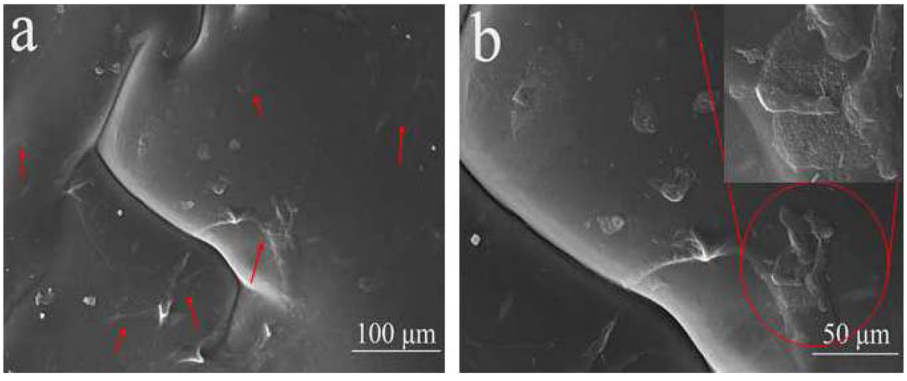

Fig. 7. SEM images of MSCs cultured 3 days on HA/collagen composite implant. (a, b — MSCs adhesion morphology and local enlarged MSCs morphology, red arrow pointed to MSCs). (For interpretation of the references to color in this figure legend, the reader is referred to the web version of this article.)

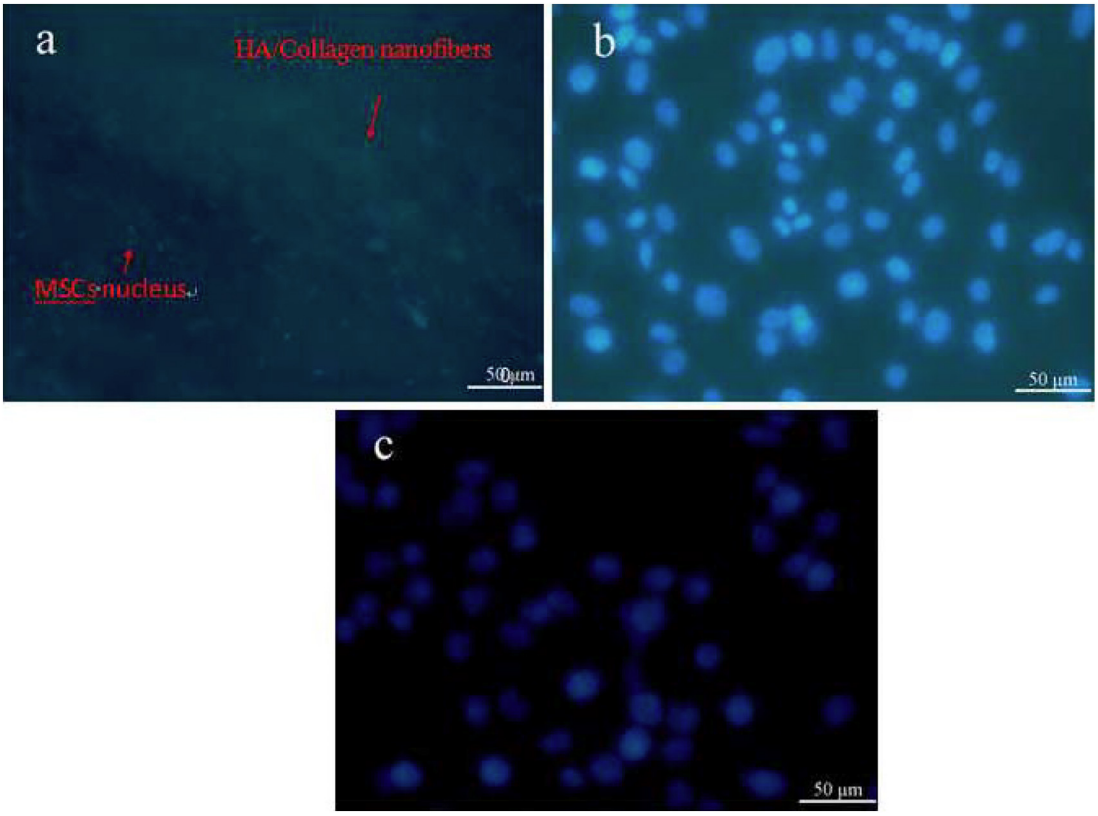

Fig. 8. Confocal images showing early attachment of MSCs on HA/collagen composite implant at 72 h after seeding. MSCs were stained with DAPI (blue, nuclei) after chemical fixation using 2.5% glutaraldehyde. (a — The blue nucleus of MSCs were distributed along the aligned nanofibers which composed the composite plant, b — MSCs nucleus on the composite plant, c — MSCs nucleus of control group). (For interpretation of the references to color in this figure legend, the reader is referred to the web version of this article.)

after biomineralization compared with the natural bone (the axial compressive strength and young modulus of human compact bone are 131–224 MPa and 17–20 GPa, respectively [58]). Further analyzed the microstructure of bone, we found the size of the motifs in natural bone is not uniform, ranging from 10 μm to 500 μm [10]. The motif size in the HA/collagen nanofiber scaffold was designed to be uniform (about 500 μm). In addition, the interlayer fibers found in natural bone motifs are arranged at different angles to each other (including parallel) [59], and the center of every bone motif has a pore of 20–100 μm. These features may affect the mechanical performance of the bone scaffold. In the future study, we will further optimize the biomimetic bone microstructure.

Technically, small micropore and micro-size motifs are not easy to construct, and converting the orientation of the fiber matrix composing the micron motifs is more difficult. The bioinspired control of structure and function is recognized as a promising strategy to enhance bone scaffold performance. Ultimately, these will be achieved by technical advancement in the future.

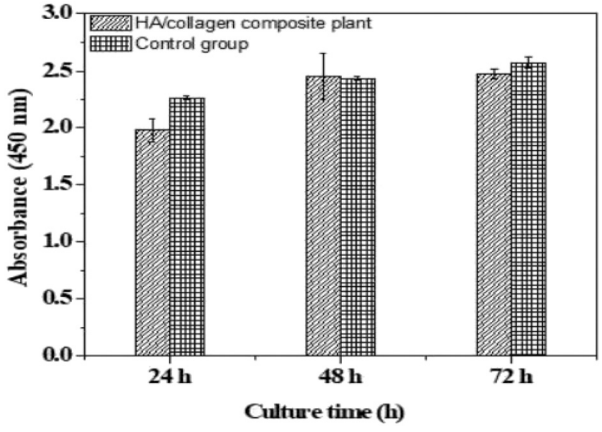

Fig. 9. CCK8 assay for assessing proliferation of MSCs cultured in leaching solution of HA/collagen composite scaffold for 24, 48 and 72 h.

4. Conclusion

We used bottom-up biomimetic bone structure synthesis from the nanoscale to the micro- and macroscopic levels to construct HA/collagen composite scaffold with a biomimetic bone Haversian microstructure. The mechanical properties of the mineralized scaffolds were improved by the double strengthening, one is a large number of newborn nano-particles HA strengthening, HA particles distributed on the scaffold microstructure; the other is the new

Table 2
Cytotoxity of HA/collagen composite implant.

Culture time	OD (450 nm)	RGR (%)	Grade
24 h	1.9781 ± 0.1044	87.41	1
48 h	2.4496 ± 0.2022	100.70	0
72 h	2.473 ± 0.0395	96.11	1
Control (24 h)	2.2631 ± 0.01745	100	
Control (48 h)	2.4326 ± 0.0146	100	
Control (72 h)	2.573 ± 0.04716	100	

chemical bonds strengthening, these bonds between HA and collagen generated within and between the nanofibrous matrix membrane of the scaffold. In addition, the scaffold maintains the fibrillar structures, large specific surface area and through pores suitable for bone tissue engineering, which are beneficial to cell growth, proliferation and material metabolism. Thus, we believe that this biomimetic bone scaffold can provide a promising application for bone tissue engineering.

Author contributions section

Tierong Bian performed data analyses and wrote the manuscript. Kang Zhao and Yufei Tang contributed to conception of the study. Qingnan Meng, Hua Jiao and Jing Luo contributed to analysis.

Acknowledgement

This work was supported by National Natural Science Foundation of China (No. 51372199).

Data availability

The raw and processed data required to reproduce these findings cannot be shared at this time due to technical limitations related to file size for CT data sets. Data is available upon request.

References

[1] S.V. Dorozhkin, Calcium orthophosphate-containing biocomposites and hybrid biomaterials for biomedical applications, J. Funct. Biomater. 6 (2015) 708–832.
[2] M. Bouler, P. Pilet, O. Gauthier, E. Verron, Biphasic calcium phosphate ceramics for bone reconstruction: a review of biological response, Acta Biomater. 53 (2017) 1–12.
[3] R. Langer, J.P. Vacanti, Tissue engineering, Science 260 (1993) 920–926.
[4] P.X. Ma, R. Zhang, G. Xiao, R. Franceschi, Fabrication of bioceramic scaffolds with pre-designed internal architecture by gel casting and indirect stereolithography techniques, J. Biomed. Mater. Res. 54 (2001) 284–293.
[5] N. Diomidis, S. Mischler, N.S. More, M. Roy, Tribo-electrochemical characterization of metallic biomaterials for total joint replacement, Acta Biomater. 8 (2012) 852–859.
[6] A.M. Ferreiraa, P. Gentilea, V. Chionoa, Collagen for bone tissue regeneration, Acta Biomater. 8 (2012) 3191–3200.
[7] A. Dey, S.K. Nandi, B. Kundu, Evaluation of hydroxyapatite and β-tricalcium phosphate microplasma spray coated pin intra-medullary for bone repair in a rabbit model, Ceram. Int. 37 (2011) 1377–1391.
[8] S. Franz, S. Rammelt, D. Scharnweber, J.C. Simon, Immune responses to implants — a review of the implications for the design of immunomodulatory biomaterials, Biomaterials 32 (28) (2011) 6692–6709.
[9] K. Zhao, Y.F. Tang, Y.S. Qin, J.Q. Wei, Porous hydroxyapatite ceramics by ice templating: freezing characteristics and mechanical properties, Ceram. Int. 37 (2) (2011) 635–639.
[10] S.L. Wu, X.M. Liu, K.W.K. Yeung, C.S. Liu, X.J. Yang, Biomimetic porous scaffolds for bone tissue engineering, Mater. Sci. Eng. R. 80 (2014) 1–36.
[11] D.F. Luo, K. Zhao, Y.N. Chen, C.F. Ma, S.X. Wu, Fabrication of interconnected spherical porous hydroxyapatite scaffold, J. Chin. Ceram. Soc. 35 (7) (2007) 368–372.
[12] S. Deville, E. Saiz, R.K. Nalla, A.P. Tomsia, Freezing as a path to build complex composites, Science 311 (2006) 515–518.
[13] U.G.K. Wegst, H. Bai, E. Saiz, A.P. Tomsia, R.O. Ritchie, Bioinspired structural materials, Nat. Mater. 14 (2015) 23–35.
[14] S. Weiner, D.H. Wagner, The material bone: structure-mechanical function relations, Annu. Rev. Mater. Sci. 28 (1998) 271–298.
[15] N. Reznikov, R. Shahar, S. Weiner, Three-dimensional structure of human lamellar bone: the presence of two different materials and new insights into the hierarchical organization, Bone 59 (2014) 93–104.
[16] H.P. Schwarcz, The ultrastructure of bone as revealed in electron microscopy of ion-milled sections, Semin. Cell Dev. Biol. 46 (2015) 44–50.
[17] J. Mitchell, A.H.V. Heteren, A literature review of the spatial organization of lamellar bone, C.R. Palevol. 15 (2016) 23–31.
[18] U.G.K. Wegst, M. Schecter, A.E. Donius, P.M. Hunger, Biomaterials by freeze casting, Phil. Trans. R. Soc. A 368 (2010) 2099–2121.
[19] S. Deville, E. Saiz, A.P. Tomsia, Ice-templated porous alumina structures, Acta Mater. 55 (2007) 1965–1974.
[20] S.J. Hollister, Porous scaffold design for tissue engineering, Nat. Mater. 4 (2005) 518–524.
[21] J.A. Lewis, Direct ink writing of 3D functional materials, Adv. Funct. Mater. 16 (2006) 2193–2204.
[22] Q.A. Fu, E. Saiz, A.P. Tomsia, Bioinspired strong and highly porous glass scaffolds, Adv. Funct. Mater. 21 (2011) 1058–1063.
[23] A.J. Wang, T. Paterson, R. Owen, C. Sherborne, J. Dugan, J.M. Li, F. Claeyssens, Photocurable high internal phase emulsions (HIPEs) containing hydroxyapatite for additive manufacture of tissue engineering scaffolds with multi-scale porosity, Mater. Sci. Eng. C 67 (2016) 51–58.
[24] S.C. Cox, J.A. Thornby, G.J. Gibbons, M.A. Williams, K.K. Mallick, 3D printing of porous hydroxyapatite scaffolds intended for use in bone tissue engineering applications, Mater. Sci. Eng. C 47 (2015) 237–247.
[25] Y. Luo, A. Lode, C. Wu, J. Chang, M. Gelinsky, Alginate/nanohydroxyapatite scaffolds with designed core/shell structures fabricated by 3D plotting and in situ mineralization for bone tissue engineering, ACS Appl. Mater. Interfaces 7 (2015) 6541–6549.
[26] A. Kumar, A.R. Akkineni, B. Basu, M. Gelinsky, Three dimensional plotted hydroxyapatite scaffolds with predefined architecture: comparison of stabilization by alginate crosslinking versus sintering, J. Biomater. Appl. 30 (2016) 1168–1181.
[27] S. Shkarina, R. Shkarin, V. Weinhardt, E. Melnik, G. Vacun, P. Kluger, K. Loza, M. Epple, S.I. Ivlev, T. Baumbach, M.A. Surmeneva, R.A. Surmenev, 3D biodegradable scaffolds of polycaprolactone with silicate containing hydroxyapatite microparticles for bone tissue engineering: high-resolution tomography and in vitro study, Sci. Rep. 8 (2018) 8907–8920.
[28] S.N. Gorodzha, A.R. Muslimov, D.S. Syromotina, A.S. Timin, N.Y. Tcvetkov, K.V. Lepik, A.V. Petrova, M.A. Surmeneva, D.A. Gorin, G.B. Sukhorukov, R.A. Surmenev, A comparison study between electrospun polycaprolactone and piezoelectric poly(3-hydroxybutyrate-co-3-hydroxyvalerate) scaffolds for bone tissue engineering, Colloid Surf. B 160 (2017) 48–59.
[29] H.E. Ying, X. Liu, X.Y. Tang, In vitro study of electrospun polycaprolactone/chitosan nano fiber membrane guided bone regeneration, Shanghai J. Stomatol. 2 (2015) 129–134.
[30] W.L. Shao, J.X. He, Q.M. Han, F. Sang, Q. Wang, L. Chen, S.Z. Cui, B. Ding, A biomimetic multilayer nanofiber fabric fabricated by electrospinning and textile technology from polylactic acid and Tussah silk fibroin as a scaffold for bone tissue engineering, Mater. Sci. Eng. C 67 (2016) 599–610.
[31] S. Kwak, A. Haider, K.C. Gupta, S. Kim, I.K. Kang, Micro/nano multilayered scaffolds of PLGA and collagen by alternately electrospinning for bone tissue engineering, Nanoscale Res. Lett. 11 (2016) 323–338.
[32] K.M. Sajesh, K. Kiran, V.N. Shantikumar, R. Jayakumar, Sequential layer-by-layer electrospinning of nano $SrCO_3$/PRP loaded PHBV fibrous scaffold for bone tissue engineering, Compos. Part B Eng. 99 (2016) 445–452.
[33] S. Deepthi, M.N. Sundaram, J.D. Kadavan, R. Jayakumar, Layered chitosan-collagen hydrogel/aligned PLLA nanofiber construct for flexor tendon regeneration, Carbohydr. Polym. 153 (2016) 492–500.
[34] H.M. Pauly, D.J. Kelly, K.C. Popata, N.A. Trujillo, N.J. Dunne, H.O. McCarthy, T.L.H. Donahu, Mechanical properties and cellular response of novel electrospun nanofibers for ligament tissue engineering: effects of orientation and geometry, J. Mech. Behav. Biomed. Mater. 61 (2016) 258–270.
[35] A.C. Tas, S.B. Bhaduri, Rapid coating of Ti6Al4V at room temperature with a calcium phosphate solution similar to 10× simulated body fluid, J. Mater. Res. 19 (2004) 2742–2749.
[36] J. Black, R. Mattson, E. Korostof, Haversian osteons: size, distribution, internal structure, and orientation, J. Biomed. Mater. Res. 8 (1974) 299–319.
[37] A. Mayya, A. Banerjee, R. Rajesh, Haversian microstructure in bovine femoral cortices: an adaptation for improved compressive strength, Mater. Sci. Eng. C 59 (2016) 454–463.
[38] T.M. Keaveny, E.F. Morgan, G.L. Niebu, Biomechanics of trabecular bone, Annu. Rev. Biomed. Eng. 3 (2001) 307–333.
[39] W.B. Lievers, S.D. Waldman, A.K. Pilkey, Minimizing specimen length in elastic testing of end-constrained cancellous bone, J. Mech. Behav. Biomed. Mater. 3 (2010) 22–30.
[40] W.B. Lievers, A.C. Petryshyn, A.S. Poljsak, Specimen diameter and "side artifacts" in cancellous bone evaluated using end-constrained elastic tension, Bone 47 (2010) 371–377.
[41] A.P. Tiwari, M.K. Joshi, J.I. Kim, A.R. Unnithan, J. Lee, C.H. Park, C.S. Kim, Bimodal fibrous structures for tissue engineering: fabrication, characterization and in vitro biocompatibility, J. Colloid Interface Sci. 476 (2016) 29–34.
[42] S. Chahala, F.S.J. Hussaina, M.M. Yusoffa, M.S.B.A. Rasadb, A. Kumar, Nanohydroxyapatite-coated hydroxyethyl cellulose/poly (vinyl) alcohol electrospun scaffolds and their cellular response, Int. J. Polym. Mater. Polym. Biomater. 66 (3) (2017) 115–122.
[43] L. Tian, Y. Chen, S.J. Min, Research on cytotoxicity of silk fibroin gel materials prepared with polyepoxy compound, J. Biomed. Eng. 24 (6) (2007) 1309–1313.
[44] D.A.C. Casadiego, M. Michael, S. Paul, A. Jorge, "Green" electrospinning of a collagen/hydroxyapatite composite nanofibrous scaffold, MRS Commun. 6 (2016) 402–407.
[45] L. Rajzer, O. Castano, E. Engel, Injectable and fast resorbable calcium phosphate cement for body-setting bone grafts, J. Mater. Sci. Mater. Med. 21 (2010) 2049–2056.
[46] A. Kumar, A.R. Akkineni, B. Basu, M. Gelinsky, Three dimensional plotted hydroxyapatite scaffolds with predefined architecture: comparison of stabilization by alginate crosslinking versus sintering, J. Biomater. Appl. 30 (2016) 1168–1181.
[47] J. Rouwkema, N.C. Rivron, C.A. van Blitterswijk, Vascularization in tissue engineering, Trends Biotechnol. 26 (2008) 434–441.
[48] K. Shin, T. Acri, S. Geary, A.K. Salem, Biomimetic mineralization of biomaterials using simulated body fluids for bone tissue engineering and regenerative medicine, Tissue Eng. A 23 (19–20) (2017) 1169–1180.
[49] Z.L. Huang, J.M. Guo, W. Liu, Y.H. Long, The Character of IR spactras of collagen and its biomineral, J. Honghe Univ. 1 (2003) 41–43.
[50] A. Kramschuster, L.S. Turng, An injection molding process for manufacturing highly porous and interconnected biodegradable polymer matrices for use as tissue engineering scaffold, J. Biomed. Mater. Res. B 92 (2) (2010) 366–376.

[51] W.E. Caler, D.R. Carte, Bone creep–fatigue damage accumulation, J. Biomech. 22 (6–7) (1989) 625–635.
[52] H.X. Zhao, W.H. Liang, A novel comby scaffold with improved mechanical strength for bone tissue engineering, Mater. Lett. 194 (2017) 220–223.
[53] K.H. Shin, J.W. Kim, Y.H. Koh, H.E. Kim, Novel self-assembly-induced 3D plotting for macro/nano-porous collagen scaffolds comprised of nanofibrous collagen filaments, Mater. Lett. 143 (2015) 265–268.
[54] B.L. Taylor, A. Limaye, J. Yarborough, J.W. Freeman, Investigating processing techniques for bovine gelatin electrospun scaffolds for bone tissue regeneration, J. Biomed. Mater. Res. B Appl. Biomater. 105 (5) (2017) 1131–1140.
[55] H. Lee, Y. Kim, S. Kim, G. Kim, Mineralized biomimetic collagen/alginate/silica composite scaffolds fabricated by a low-temperature bio-plotting process for hard tissue regeneration: fabrication, characterisation and in vitro cellular activities, J. Mater. Chem. B 2 (2014) 5785–5798.
[56] H.W. Frost, Perspective: bone's mechanical usage windows, Bone Miner. 19 (3) (1993) 257–271.
[57] N. Nseir, O. Regev, T. Kaully, J. Blumenthal, S. Levenberg, E. Zussman, Biodegradable scaffold fabricated of electrospun albumin fibers: mechanical and biological characterization, Tissue Eng. Part C Methods 19 (2012) 257–264.
[58] N. Li, G. Chen, J. Liu, Y. Xia, H. Chen, H. Tang, F. Zhang, N. Gu, Effect of surface topography and bioactive properties on early adhesion and growth behavior of mouse preosteoblast MC3T3-E1 cells, ACS Appl. Mater. Interfaces 6 (2014) 17134–17143.
[59] P.C. Liliana, L.E. Magda, E.R.V. Jaime, Scaffold design for bone regeneration, J. Nanosci. Nanotechnol. 14 (1) (2014) 15–56.